



Published in final edited form as:

J Endocrinol. 2019 August ; 242(2): 159–172. doi:10.1530/JOE-19-0126.

Endothelial adenosine kinase deficiency ameliorates diet-induced insulin resistance

Jiean Xu^{1,2}, Qiuhua Yang^{1,2}, Xiaoyu Zhang^{1,2}, Zhiping Liu^{1,2}, Yapeng Cao^{1,2}, Lina Wang^{1,2}, Yaqi Zhou^{1,2}, Xianqiu Zeng^{1,2}, Qian Ma^{1,2}, Yiming Xu^{2,3}, Yong Wang^{2,4}, Lei Huang⁵, Zhen Han⁵, Tao Wang⁵, David Stepp², Zsolt Bagi⁶, Chaodong Wu⁷, Mei Hong^{1,*}, Yuqing Huo^{2,*}

¹Drug Discovery Center, State Key Laboratory of Chemical Oncogenomics, Key Laboratory of Chemical Genomics, Peking University Shenzhen Graduate School, Shenzhen 518055, China.

²Vascular Biology Center, Department of Cellular Biology and Anatomy, Medical College of Georgia, Augusta University, Augusta, GA 30912, USA.

³School of Basic Medical Sciences, Guangzhou Medical University, Guangzhou 511436, China.

⁴College of Basic Medicine, Chengdu University of Traditional Chinese Medicine, Chengdu 610075, China.

⁵Department of Cardiovascular Surgery, Peking University Shenzhen Hospital, Shenzhen 518036, China.

⁶Department of Physiology, Medical College of Georgia, Augusta University, Augusta, GA 30912, USA.

⁷Department of Nutrition and Food Science, Texas A&M University, College Station, TX 77840, USA.

Abstract

Insulin resistance-related disorders are associated with endothelial dysfunction. Accumulating evidence has suggested a role for adenosine signaling in the regulation of endothelial function. Here, we identified a crucial role of endothelial adenosine kinase (ADK) in the regulation of insulin resistance. Feeding mice with a high-fat diet (HFD) markedly enhanced expression of endothelial Adk. Ablation of endothelial *Adk* in HFD fed mice improved glucose tolerance and insulin sensitivity, decreased hepatic steatosis, adipose inflammation, and adiposity, which were associated with improved arteriole vasodilation, decreased inflammation and increased adipose angiogenesis. Mechanistically, ADK inhibition or knockdown in Human Umbilical Vein

Corresponding author: Yuqing Huo, MD, PhD, Vascular Biology Center, Department of Cellular Biology and Anatomy, Medical College of Georgia, Augusta University., Phone: 706-721-4414 (Office), Fax: 706-721-9799 (VBC), yhuo@augusta.edu, Mei Hong, MD, PhD, State Key Laboratory of Chemical Oncogenomics, Peking University Shenzhen Graduate School, Phone: +86-755-2153-9221 (Office), Fax: +86-755-2603-3061, meihong.sz@pku.edu.cn.

*equally contributed to this study

Author contribution statement

J.X., L.H., Z.H., T.W., D.S., Z.B., C.W., M.H. and Y.H. designed the research; J.X., Q.Y., X.Z., Z.L., Y.C., L.W., Y.Z., X.Z., Q.M., Y.X. and Y.W. performed experiments; J.X., Q.Y., X.Z. and Y.H. analyzed data; J.X., C.W., M.H. and Y.H. wrote and revised the manuscript; and D.S., L.H., C.W., Z.B. and M.H. provided the reagents or materials and participated in experimental design. M.H. and Y.H. had primary responsibility for the final content. All authors read and approved the final manuscript.

Declaration of interest

The authors declare that there is no conflict of interest that could be perceived as prejudicing the impartiality of the research reported.

Endothelial Cells (HUVECs) elevated intracellular adenosine level and increased endothelial nitric oxide synthase (NOS3) activity, resulting in an increase in nitric oxide (NO) production. Antagonism of adenosine receptor A2b abolished *ADK*-knockdown- enhanced NOS3 expression in HUVECs. Additionally, increased phosphorylation of NOS3 in *ADK*-knockdown HUVECs was regulated by an adenosine receptor-independent mechanism. These data suggest that *Adk*-deficiency-elevated intracellular adenosine in endothelial cells ameliorates diet-induced insulin resistance and metabolic disorders, and this is associated with an enhancement of NO production caused by increased NOS3 expression and activation. Therefore, ADK is a potential target for prevention and treatment of metabolic disorders associated with insulin resistance.

Keywords

Obesity; Insulin resistance; Endothelium; Adenosine kinase; Nitric oxide

Introduction

Vascular endothelium plays a crucial role in the regulation of metabolic homeostasis, and dysregulated endothelial function induces the development of metabolic disorders (Graupera and Claret 2018; Pi, et al. 2018). Multiple molecules/pathways in endothelial cells have been identified to directly modulate systemic metabolism, including the nitric oxide (NO) system regulated by endothelial nitric oxide synthase (NOS3), insulin cascade (INSR and IRS2), angiogenic signals (VEGFR1) and transcription factors (P53 and NFKBIA) (Duplain, et al. 2001; Hasegawa, et al. 2012; Konishi, et al. 2017; Kubota, et al. 2011; Seki, et al. 2018; Yokoyama, et al. 2014). Dysregulation of these pathways results in insulin resistance-associated metabolic perturbations.

Accumulating evidence highlights a critical role for adenosine signaling in the development of insulin resistance (Antonioli, et al. 2015; Pardo, et al. 2017). Adenosine signaling is also closely associated with endothelial inflammation, angiogenesis and vascular dilation (Adair 2004; Bouma, et al. 1996; Smits, et al. 1995). Adenosine regulates the function of cells through signaling to its four receptors including A1, A2a, A2b, and A3, or through receptor-independent mechanisms (Boison 2013; Borea, et al. 2016). Adenosine is produced by the dephosphorylation of adenosine monophosphate (AMP), a reaction catalyzed by 5'-nucleotidase intracellularly or ecto-5'-nucleotidase extracellularly (Borea et al. 2016). In addition to AMP degradation, intracellular adenosine can also be formed through hydrolysis of S-adenosylhomocysteine (SAH) by SAH hydrolase (Borea et al. 2016). Adenosine is catabolized to AMP via adenosine kinase (ADK) or inosine via adenosine deaminase (ADA) (Borea et al. 2016). ADK is a principal intracellular enzyme in maintaining intracellular adenosine homeostasis (Boison 2013). Previous studies demonstrated a beneficial role of ADK inhibition in experimental diabetes by regulating proliferation of β -cells and reduced blood glucose level *in vivo* (Annes, et al. 2012; Navarro, et al. 2017; Pye, et al. 2014). However, it remains unclear whether elevated endothelial intracellular adenosine via ADK inactivation can regulate endothelial function and protect mice from diet-induced insulin resistance.

In the current study, we examined the effects of endothelial *Adk* deficiency-elevated intracellular adenosine on diet-induced insulin resistance. We found that endothelial-specific *Adk* deficiency had a glucose-lowering effect in mice fed a chow diet (CD) and protected mice from high-fat-diet (HFD)-induced insulin resistance and metabolic syndrome, which was associated with an enhancement of NO production by increased NOS3 phosphorylation and protein expression.

Materials and methods

Animal experiments

All mouse experiments were approved by the Institutional Animal Care and Use Committee of Peking University Shenzhen Graduate School and Augusta University. The generation of *Adk*^{flox/flox}; *Cdh5-Cre* (*Adk*^{VEC}) mice and their littermate control *Adk*^{flox/flox} (*Adk*^{WT}) mice has been described previously (Xu, et al. 2017b). Six-week-old *Adk*^{WT} and *Adk*^{VEC} male mice were fed *ad libitum* either a normal chow diet (CD) or a high-fat diet (HFD) (D12492, Research Diet, New Brunswick, NJ, USA) for 12 weeks followed by analysis of insulin sensitivity.

Evaluation of energy homeostasis

Food intake, locomotor activity and energy expenditure were determined with Comprehensive Lab Animal Monitoring System (Columbus Instruments, Columbus, OH, USA). Body composition of lean and fat mass was determined by nuclear magnetic resonance (MiniSpec LF90II TD-NMR Analyzer, Bruker, Billerica, MA, USA). Epididymal fat depots and liver were dissected and weighed during necropsy.

Evaluation of glucose homeostasis

Blood glucose and insulin levels from tail vein blood samples were measured at 16 h after fasting using a glucometer (OneTouch UltraEasy, Johnson & Johnson, New Brunswick, NJ, USA) and a mouse insulin ELISA kit (80-INSMS-E01, ALPCO, Salem, NH, USA) after fasting for 16 h at the indicated ages. For glucose tolerance test (GTT), the mice were fasted for 6 hours and received an intraperitoneal injection of D-glucose (2 g/kg; G8270, Sigma-Aldrich, St. Louis, MO, USA). Tail vein blood samples were collected at 0, 30, 60, 90 and 120 min after injection and glucose was measured with a glucometer. For insulin tolerance test (ITT), the mice were fasted for 4 hours and given insulin (HI0219, Lilly, Indianapolis, IN, USA) at 1 unit/kg (mice fed a CD) or 0.75 unit/kg (mice fed an HFD) by intraperitoneal injection. Tail vein blood samples were collected at the indicated times for blood glucose measurement by a glucometer.

Insulin signaling studies *in vivo*

Mice fed an HFD for 12 weeks were fasted for 4 h and anesthetized with an intraperitoneal injection of ketamine (100 mg/kg) and xylazine (10 mg/kg), and then received insulin (1 unit/kg) or saline by intravenous injection into the inferior vena cava. Five minutes after injection, samples of liver, epididymal adipose and quadriceps muscle were removed quickly, immediately frozen in liquid nitrogen, and stored at -80°C for analysis of Akt phosphorylation with Western blotting.

Skeletal muscle arteriolar vasodilation *in vitro*

Videomicroscopy of isolated skeletal muscle arterioles was performed as previously described (Bagi, et al. 2005). Briefly, isolated gracilis muscle arterioles were cannulated at both ends with glass micropipettes and pressurized (70 mmHg) with the use of hydrostatic pressure reservoirs. Changes in arteriolar diameter were measured with a videocaliper (Colorado Instruments, Colorado Springs, CO, USA) in response to cumulative concentrations of acetylcholine (10^{-10} – 10^{-6} M; A6625, Sigma-Aldrich, St. Louis, MO, USA) in the absence or presence of L-NAME (0.2 mM; N5751, Sigma-Aldrich, St. Louis, MO, USA).

Hepatic triglyceride measurement

After fasting for 4 h, mice were euthanized and liver tissues were collected from 12-week HFD-fed *Adk*^{WT} and *Adk*^{VEC} mice, weighed and homogenized in RIPA lysis buffer (R0278, Sigma-Aldrich, St. Louis, MO, USA) on ice. Lipids in the liver homogenate were extracted in a mixture of chloroform and methanol (2:1) on a shaker at 100 rpm for 12 h at 4 °C, then washed with 0.9% NaCl and centrifuged at 2000g for 20 min at 4 °C. The organic layer was collected, evaporated and redissolved in isopropanol. Liver triglyceride concentrations were assayed using a triglyceride assay kit (A110–1, Nanjing Jiancheng Bioengineering Institute, Nanjing, China) according to the manufacturer's instructions.

Adipose stromal vascular fraction isolation and flow cytometry analysis

Epididymal adipose tissue was collected and digested on a shaker at 37 °C for 45 minutes in DMEM medium (A14430–01, Gibco, Grand Island, NY, USA) containing 1mg/ml collagenase D (COLLD-RO, Sigma-Aldrich, St. Louis, MO, USA), 10 mg/ml BSA, 0.5 mM CaCl₂ and 15 mM HEPES. After centrifugation at 500 g for 5 min at 4 °C, stromal vascular fraction (SVF) pellets were incubated in 100 µl FACS buffer (0.1% BSA in PBS, pH 7.4) containing 2 µg Fc block (553141, BD Biosciences, San Jose, CA, USA) for 15 min at room temperature, and then stained with appropriate fluorescently labeled primary antibodies or isotype controls listed in Supplementary Table 1 for 30 min at 4 °C in the dark. The cells were resuspended in 0.5 ml FACS buffer containing 1% PFA. SVF cells were analyzed using FACSCalibur (BD Biosciences, San Jose, CA, USA) and FlowJo (TreeStar, Ashland, OR, USA).

Histological analysis

Samples of liver and adipose were fixed and embedded in paraffin according to a standard protocol. 5 µm sections of liver or adipose were sectioned and stained with hematoxylin and eosin (H&E) routinely. Mac-2 immunohistochemical (IHC) staining of adipose tissue was performed as previously described (Xu, et al. 2017a). For Adk immunofluorescence (IF) staining in adipose vessels, sections were incubated with anti-Adk (10 µg/ml, A304–280A, Bethyl Laboratories, Montgomery, TX, USA) and anti-Pecam1 (2 µg/ml, DIA-310, Dianova, Hamburg, Germany), then incubated with Alexa Fluor 594-labeled goat anti-rabbit IgG (1:250, A11012, Molecular Probes, Grand Island, NY, USA) and Alexa Fluor 488-labeled goat anti-mouse IgG (1:250, A11001, Molecular Probes, Grand Island, NY, USA). For isolectin GS-IB₄ IF staining in adipose tissue, whole-mount staining was performed as

previously described (Xue, et al. 2010). Briefly, the distal epididymal adipose tissue samples were excised from mice and fixed in 4% PFA overnight at 4 °C. Samples were digested with proteinase K (20 µg/ml) for 5 min at room temperature and incubated with methanol for 30 min at room temperature. After blocking with 3% blocking buffer overnight at 4 °C, samples were stained on a shaker overnight at 4 °C with Alexa-594 labeled Griffonia simplicifolia isolectin B4 (1:200, I21413, Invitrogen, Grand Island, NY, USA). After washing thoroughly with PBST, samples were immersed in mounting medium (H-1000, Vector Laboratories, Burlingame, CA, USA), imaged with a confocal microscope (Zeiss 780 Upright Confocal, Carl Zeiss, Oberkochen, Germany), and analyzed quantitatively using an Adobe Photoshop program.

Cell culture and treatments

Human umbilical vein endothelial cells (HUVECs) were cultured as previously described (Xu et al. 2017b). In some experiments, HUVECs were incubated with 0.1–0.5 mM palmitic acid (PA, P5585, Sigma-Aldrich, St. Louis, MO, USA), 2–20 µM ABT702 (2372, Tocris Bioscience, Bristol, United Kingdom), 5 µM ZM241385 (1036, Tocris Bioscience, Bristol, United Kingdom), 5 µM MRS1754 (2752, Tocris Bioscience, Bristol, United Kingdom) or 10 µM ITU (1745, Tocris Bioscience, Bristol, United Kingdom). Adenoviral transduction of HUVECs was performed as previously described (Xu et al. 2017b). Palmitate-BSA complex was prepared as previously described (Maloney, et al. 2009).

Analysis of nitric oxide (NO) release

The measurement of NO release was performed using a Sievers NOA 280i chemiluminescence analyzer (Analytix, Sunderland, UK) as previously described (Ahmed, et al. 1997). Briefly, 100 µl of supernatant were injected into a nitrogen-purge vessel containing a 1% solution of sodium iodide in glacial acetic acid. The output was recorded using a Labchart program (ADInstruments, Colorado Springs, CO, USA) and the area under the curve was converted to picomole NO using a calibration curve constructed after the analysis of a series of sodium nitrite standards ranging from 2.5 to 100 pmol.

Measurement of intracellular adenosine concentration

The adenosine concentrations were measured using reverse-phase HPLC as previously described (Xu et al. 2017a).

Western blot analysis

Western blot was performed as previously described (Liu, et al. 2017). The antibodies used are listed in Supplementary Table 2. Band densities were quantified using ImageJ (National Institutes of Health, Bethesda, MD, USA).

Quantitative PCR (qPCR) analysis

Quantitative PCR was performed as previously described (Xu et al. 2017b). The primers used are listed in Supplementary Table 3. Quantification of relative gene expression was calculated with the 2^{-CT} method using the internal control *Gapdh* or *18S* rRNA.

Statistical analysis

Statistical analysis was performed with GraphPad Prism 7 software (GraphPad, La Jolla, CA, USA). The data are presented as the means \pm s.e.m. Statistical comparisons were performed using two-tailed unpaired Student's *t*-test or one-way analysis of variance (ANOVA) followed by Bonferroni's post-hoc test when appropriate. Differences were considered significant at $P < 0.05$, and statistical significance was defined as follows: * $P < 0.05$, ** $P < 0.01$, *** $P < 0.001$ and **** $P < 0.0001$.

Results

The expression and activity of endothelial adenosine kinase are enhanced under metabolic stress

We examined the expression of Adk in adipose tissue of HFD-fed mice by using qPCR and WB, and found that the expression of Adk was increased at both protein and mRNA levels in adipose tissue in HFD-fed mice compared with that of CD-fed mice (Fig. 1A and B). These results are consistent with earlier finding that the activity of Adk is increased in adipose tissue in obese mice as compared to their lean littermates (Green, et al. 1981). To further determine the influence of metabolic stress on the expression of endothelial ADK, we analyzed the levels of endothelial Adk in adipose from mice fed with HFD. In an immunostaining assay, endothelial Adk expression was increased on the vascular endothelium of HFD-fed mice compared with that of CD-fed mice (Fig. 1C). We then examined the expression and function of endothelial ADK using an *in vitro* assay. HUVECs were treated with palmitic acid (PA), and the efficacy of PA treatment on endothelial cells (ECs) were evidenced with the increased expression of *ICAM-1*, the critical marker of endothelial activation (Supplementary Fig. 1A and B). PA treatment led to upregulation of ADK at the protein level in HUVECs, resulting in decreased level of intracellular adenosine compared with vehicle-treated cells (Fig. 1D and E). The increased ADK protein level in PA-treated HUVECs was due to an increased mRNA level, which was demonstrated by qPCR assay (Fig. 1F and G). Together, these findings suggested that metabolic stress reprograms the expression of ADK and this may be a critical link in the development of metabolic syndrome.

Endothelial *Adk* deficiency modestly alters the metabolic phenotype of mice fed a chow diet

To investigate the role of endothelial Adk in metabolic homeostasis in mice, we generated endothelial Adk-deficient mice (*Adk*^{VEC}) and fed these mice and their littermate controls (*Adk*^{WT} mice) a chow diet and examined metabolic parameters in these mice. The body weight of *Adk*^{VEC} mice was slightly higher than *Adk*^{WT} mice after 12 weeks of CD (Fig. 2A). However, *Adk*^{VEC} mice had a significantly lower body fat content than *Adk*^{WT} mice in the measurement with NMR (Fig. 2B). This was in line with the lower weight of epididymal white adipose tissue (eWAT) in *Adk*^{VEC} mice than *Adk*^{WT} mice (Fig. 2C). The content of lean mass is higher in *Adk*^{VEC} mice compared to that of *Adk*^{WT} mice, although this increase does not reach statistical significance (Fig. 2B). However, this may explain the slight increase in body weight in *Adk*^{VEC} mice following 12 weeks of CD feeding (Fig. 2A). *Adk*^{VEC} mice had a significantly lower fasting blood glucose level than *Adk*^{WT} mice

whereas their levels of fasting serum insulin were similar (Fig. 2D and Supplementary Fig 2A). Despite that the fasting blood glucose of *Adk*^{VEC} mice was lower than that of *Adk*^{WT} mice, elevation of blood glucose after intraperitoneal glucose administration and the glucose-lowering effect of insulin did not differ significantly between *Adk*^{VEC} mice and *Adk*^{WT} mice (Fig. 2E and F). In the Comprehensive Lab Animal Monitoring System, no differences in food intake, locomotor activity, oxygen consumption, carbon dioxide production, and respiratory exchange ratio or energy expenditure were found between *Adk*^{VEC} and *Adk*^{WT} mice (Supplementary Fig. 2B–G). These results indicate that endothelial *Adk* deficiency causes a very modest metabolic change in mice on CD.

Endothelial *Adk* deficiency protects mice from high fat diet (HFD)-induced insulin resistance

When challenged with an HFD, *Adk*^{VEC} mice displayed resistance to HFD-induced body-weight gain with an approximately 10% lower average body weight than that of *Adk*^{WT} mice following four weeks of HFD feeding (Fig. 3A). *Adk*^{VEC} mice showed a lower body fat content by NMR measurement (Fig. 3B) and a higher percentage of lean mass than *Adk*^{WT} mice (Supplementary Fig. 3A). Also, *Adk*^{VEC} mice had a significant reduction in the weight of eWAT compared with *Adk*^{WT} mice (Supplementary Fig. 3B). Consistent with the above results, using the Comprehensive Lab Animal Monitoring System, *Adk*^{VEC} mice had a modest increase in locomotor activity, oxygen consumption and carbon dioxide production without a significant alteration in food intake, respiratory exchange ratio and energy expenditure compared with *Adk*^{WT} mice after the 12-week HFD feeding (Supplementary Fig. 3C–H). Moreover, *Adk*^{VEC} mice exhibited significantly decreased blood glucose level compared to *Adk*^{WT} mice over 12 weeks of HFD feeding (Fig. 3C). In addition, fasting blood insulin levels were also dramatically reduced in *Adk*^{VEC} mice compared to that in *Adk*^{WT} mice after an HFD (Fig. 3D). In agreement with these observations, *Adk*^{VEC} mice exhibited improved glucose clearance in GTTs, as well as improved insulin sensitivity in ITTs compared with *Adk*^{WT} mice (Fig. 3E and F). This increased insulin sensitivity in *Adk*^{VEC} mice was further confirmed by Western blotting assays with samples from major metabolic organs, in which the levels of insulin-stimulated Akt Ser473 phosphorylation in liver, eWAT and muscle were higher in *Adk*^{VEC} mice than *Adk*^{WT} mice (Fig. 3G–I). These results indicate that endothelial *Adk* deficiency attenuates HFD-induced systemic insulin resistance by improving insulin sensitivity in liver, eWAT and skeletal muscle.

Endothelial *Adk* deficiency attenuates HFD-induced hepatic steatosis

Metabolic alterations in livers of HFD-fed *Adk*^{VEC} mice were further characterized. The liver of *Adk*^{VEC} mice was smaller in size than that of *Adk*^{WT} mice (Fig. 4A). The same change was seen in the ratio of liver weight to body weight (Fig. 4B). Histological examination of liver sections showed that the hepatic lipid accumulation was significantly reduced in *Adk*^{VEC} mice compared to *Adk*^{WT} mice (Fig. 4C). This was further confirmed by the measurement of liver triglyceride content (Fig. 4D). The expression of hepatic lipogenesis- and β -oxidation-related genes was not significantly different between livers of *Adk*^{VEC} mice and those of *Adk*^{WT} mice after feeding of HFD (Supplementary Fig. 3I). However, compared with *Adk*^{WT} mice, *Adk*^{VEC} mice showed a significant decrease in the

expression of the proinflammatory cytokines *Tnfa* and *Ccl2*, and a marked increase in *Mrc1*, a marker of M2 macrophages in the liver (Fig. 4E and F). Collectively, these results suggest that endothelial *Adk* deficiency attenuates HFD-induced hepatic steatosis and hepatic insulin resistance through reduction of hepatic inflammation.

Endothelial *Adk* deficiency ameliorates HFD-induced adipose inflammation and endothelial dysfunction

As chronic adipose inflammation plays a critical role in the pathogenesis of HFD-induced systemic insulin resistance, we histologically examined the sections of eWAT and found that the HFD-induced crown-like structure formation was reduced in *Adk*^{VEC} mice compared to *Adk*^{WT} mice (Fig. 5A and B). Consistently, immunostaining with Mac-2 antibody showed that macrophage infiltration in eWAT of HFD-fed *Adk*^{VEC} mice was much lower than that of HFD-fed *Adk*^{WT} mice (Fig. 5A and C). Furthermore, FACS analysis of macrophage populations in SVF cells of eWAT revealed smaller proportions of CD11b⁺F4/80⁺ macrophages and a lower ratio of M1-like CD11b⁺F4/80⁺CD11c⁺ cells to M2-like CD11b⁺F4/80⁺CD206⁺ cells in HFD-fed *Adk*^{VEC} mice than in HFD-fed *Adk*^{WT} mice (Fig. 5D–H). Finally, compared with HFD-fed *Adk*^{WT} mice, HFD-fed *Adk*^{VEC} mice showed a significant decrease in the expression of inflammatory genes, including *Ccl2*, *Il6*, *Adgre1* and *Icam1*, and a considerable increase in the levels of *Adipoq* and *Pecam1* in the eWAT (Fig. 5I and J). These results suggest that endothelial *Adk* deficiency attenuates inflammation and increases angiogenesis in adipose tissue of HFD-fed *Adk*^{VEC} mice.

Consistently, immunostaining of whole mount adipose tissue with isolectin GS-IB₄ showed that the vasculature density in eWAT was significantly increased, whereas adipogenic/angiogenic cell cluster (AACC) numbers were markedly reduced in HFD-fed *Adk*^{VEC} mice compared with HFD-fed *Adk*^{WT} mice (Fig. 6A). Moreover, the levels of NOS3 protein and its phosphorylation in eWAT were also significantly increased in HFD-fed *Adk*^{VEC} mice compared with HFD-fed *Adk*^{WT} mice (Fig. 6B). In addition, in arterioles isolated from skeletal muscle, impaired endothelium-dependent relaxation in response to acetylcholine (ACh), a physiological NOS3 activator, was improved in HFD-fed *Adk*^{VEC} mice compared with HFD-fed *Adk*^{WT} mice. This improved arterial relaxation in HFD-fed *Adk*^{VEC} mice is partially abolished by N ω -nitro-L-arginine methyl ester (L-NAME) (Fig. 6C). Finally, we also found that the phosphorylation of NOS3 in liver and vessel density in adipose tissue were significantly increased in *Adk*^{VEC} mice compared to *Adk*^{WT} mice fed a chow diet (Supplementary Fig 3J and K).

Elevated intracellular adenosine promotes endothelial NO production *in vitro*

Since endothelial *Adk* deficiency increased NOS3 activity *in vivo*, we next investigated the mechanisms involved in the regulation of endothelial NOS3/NO pathway by ADK inhibition *in vitro*. We first examined the effects of ADK knockdown (KD) by adenovirus shADK on NOS3/NO signaling in HUVECs. Endothelial ADK KD significantly increased the levels of intracellular adenosine (Fig 7A–C), NOS3 phosphorylation and NOS3 protein (Fig 7D), and NO production (Fig 7E). Furthermore, ADK KD-mediated upregulation of NOS3 protein was compromised by blockade of ADORA2B whereas the phosphorylation of NOS3 was not disturbed by blockade of ADORA2A, ADORA2B or both, which was associated with

increased phosphorylation of AKT (Fig 7F). Consistently, ITU, an ADK inhibitor, significantly increased the phosphorylation of NOS3 and the level of NOS3 protein (Fig. 8A). ABT702, another ADK inhibitor, was able to significantly increase endothelial intracellular adenosine levels (Fig 8B), increase the phosphorylation of NOS3 (Fig. 8C), and increase NO production in a dose-dependent manner (Fig. 8D), as well as significantly increase the phosphorylation of vasodilatory-stimulated phospho-protein (VASP) (Fig. 8E), a downstream mediator of NO signaling. In addition, endothelial ADK KD protected HUVECs from PA-induced decreased AKT phosphorylation and increased ICAM-1 expression (Supplementary Fig. 4A and B).

Together, endothelial ADK deficiency-elevated intracellular adenosine enhances NO production through adenosine receptor dependent and independent pathways and ameliorates HFD-induced insulin resistance in mice (Fig. 8F).

Discussion

In the present study, we demonstrated the effect of endothelial *Adk* in the regulation of insulin resistance. Deletion of endothelial *Adk* reduces diet-induced obesity and insulin resistance. Alleviation of insulin resistance in *Adk*^{VEC} mice was demonstrated by decreased levels of fasting blood glucose and fasting serum insulin and improved glucose tolerance and insulin tolerance tests. This improved metabolic phenotype is associated with increased NOS3 activity in endothelial cells with deficiency/inhibition of ADK.

Metabolic stress regulates endothelial adenosine signaling via reprogramming adenosinergic genes. Extensive studies have been reported on the effect of adenosine signaling in metabolic cells and leukocytes in metabolic disorders (Antonioli et al. 2015; Csoka, et al. 2014). However, it remains elusive on the role of endothelial adenosine signaling in regulation of metabolic syndrome. ADK is a principal intracellular enzyme in metabolizing intracellular adenosine and subsequent adenosine signaling (Boison 2013), the effect of endothelial ADK on modulation of metabolic syndrome has not been studied yet. In the milieu of *in vitro* metabolic syndrome, PA was used to mimic the stimulation of free fatty acids on endothelium *in vivo*. Our results reveals that endothelial *ADK* is the most significantly upregulated adenosinergic gene in response to PA treatment (Supplementary Fig 1C). It has been reported that *Adk* can be upregulated in lymphocytes in response to insulin treatment via the MAPK pathway (Pawelczyk, et al. 2003). Therefore, increased *Adk* expression in endothelial cells may be attributed to an enhanced MAPK pathway under insulin resistance condition (Gogg, et al. 2009; Gustavo Vazquez-Jimenez, et al. 2016; Mather, et al. 2013). In addition, upregulation of ADK in endothelial cells may also be due to inflammatory stimuli under metabolic stress; our previous study has shown that endothelial ADK is increased in response to treatment with proinflammatory cytokines (Luan, et al. 2013; Wahlman, et al. 2018; Xu et al. 2017a).

Endothelial *Adk* knockout (KO)-increased endothelial NOS3 activity protects against diet-induced insulin resistance. It has been well accepted that preserved endothelial homeostasis protects mice from diet-induced metabolic syndrome (Graupera and Claret 2018; Pi et al. 2018). For example, deficiency of endothelial NOS3 exacerbates, while enhanced activity of

NOS3 improves, diet-induced metabolic stress including hepatic steatosis, adiposity and insulin resistance (Cook, et al. 2004; Kashiwagi, et al. 2013; Lee, et al. 2015). This has been associated with NO-regulated endothelial function, adipose inflammation, as well as macrophage polarization (Handa, et al. 2011; Kubota et al. 2011; Lee et al. 2015). In the current study, HFD-induced proinflammatory gene expression in the liver and adipose tissue was decreased in *Adk*^{VEC} mice. Enhanced M2 macrophage polarization in the adipose tissue also occurred in HFD-fed *Adk*^{VEC} mice. A further study demonstrated better dilation in response to ACh stimulation in arterioles isolated from HFD-fed *Adk*^{VEC} mice, and this is significantly diminished by treatment with NOS3 inhibitor. Therefore, our findings on decreased insulin resistance in HFD-fed *Adk*^{VEC} mice, at least in part, are associated with enhanced NOS3 activity, although increased vascularization in adipose tissue may also contribute to the reduced adipose tissue inflammation in HFD-fed *Adk*^{VEC} mice.

ADK deficiency/inhibition enhances endothelial NOS3/NO signaling through multiple pathways. Genetic and pharmacological inhibition of endothelial ADK increased intracellular adenosine and then increased NO production. This is due to increased NOS3 activity evidenced by the increased levels of NOS3 phosphorylation and NOS3 protein. The increased NOS3 protein level in this study is in line with our previous study in which the increased mRNA level of *NOS3* in *ADK* KD HUVECs is reported (Xu et al. 2017b). Our previous study also shows that endothelial ADK KD increases the level of *ADORA2B* (Xu et al. 2017b). In this study we have found that *ADORA2B* modulates NOS3 expression since, in *ADK* KD HUVECs, the enhanced expression of NOS3 was abrogated by blockade of *ADORA2B*. This observation is in agreement with the recent study from Du et al. in which adenosine receptor agonist NECA upregulates the levels of endothelial NOS3 at both mRNA and protein levels through *ADORA2B* (Du, et al. 2015). Interestingly, the enhanced phosphorylation of NOS3 is not regulated by *ADORA2B*. Our previous study showed that ADK deficiency-elevated intracellular adenosine inhibited methylation of the promoters of a series of pro-angiogenic genes, especially for *VEGFR2* (Xu et al. 2017b). Likely, the consequent increased *VEGFR2*/*AKT* signaling participates in NOS3 phosphorylation in ADK-deficient endothelial cells.

Other possible mechanisms, such as the anti-inflammatory effects of endothelial *Adk* deficiency, may also contribute to the alleviated adipose inflammation and systematic insulin resistance in HFD-fed *Adk*^{VEC} mice. Our previous study has shown that the deletion of *Adk* in endothelium reduces leukocyte rolling and adhesion on the endothelium in response to Tnfa treatment *in vivo* (Xu et al. 2017a). Therefore, it is very likely that decreased adhesion molecule expression in *Adk*-deficient endothelium upon inflammatory stimulation contributes to the decreased macrophage infiltration in adipose tissue observed in the current study.

In summary, our findings demonstrate that inactivation of endothelial ADK can regulate glucose homeostasis and insulin sensitivity via improved endothelial function and angiogenesis. A recent study has shown that deletion of *Adk* in mouse pancreatic β -cells also protects against HFD-induced glucose intolerance through increased β -cell replication and mass (Navarro et al. 2017). Although much work is required to further study the role of ADK in other types of cells in the regulation of metabolic syndrome, it is very likely that

regulation of ADK is a potential therapeutic strategy for the treatment of insulin resistance-associated metabolic disorders.

Supplementary Material

Refer to Web version on PubMed Central for supplementary material.

Acknowledgments

Funding

This work was supported in part or in whole by grants from the Shenzhen Science and Technology Innovation Committee (JCYJ20160506170316776, JCYJ20170810163238384, JCYJ20170412150405310, JCYJ20160525154531263, and JSGG20160608091824706), Guangdong Natural Science Foundation (2014A030312004), National Natural Science Foundation of China (81870324), American Heart Association (16GRNT30510010), and the National Institutes of Health (R01HL134934, R01DK095862 and R01 HL142097).

References

- Adair TH 2004 An emerging role for adenosine in angiogenesis. *Hypertension* 44 618–620. [PubMed: 15381681]
- Ahmed A, Dunk C, Kniss D & Wilkes M 1997 Role of VEGF receptor-1 (Flt-1) in mediating calcium-dependent nitric oxide release and limiting DNA synthesis in human trophoblast cells. *Lab Invest* 76 779–791. [PubMed: 9194854]
- Annes JP, Ryu JH, Lam K, Carolan PJ, Utz K, Hollister-Lock J, Arvanites AC, Rubin LL, Weir G & Melton DA 2012 Adenosine kinase inhibition selectively promotes rodent and porcine islet beta-cell replication. *Proc Natl Acad Sci U S A* 109 3915–3920. [PubMed: 22345561]
- Antonoli L, Blandizzi C, Csoka B, Pacher P & Hasko G 2015 Adenosine signalling in diabetes mellitus—pathophysiology and therapeutic considerations. *Nat Rev Endocrinol* 11 228–241. [PubMed: 25687993]
- Bagi Z, Erdei N, Toth A, Li W, Hintze TH, Koller A & Kaley G 2005 Type 2 diabetic mice have increased arteriolar tone and blood pressure: enhanced release of COX-2-derived constrictor prostaglandins. *Arterioscler Thromb Vasc Biol* 25 1610–1616. [PubMed: 15947245]
- Boison D 2013 Adenosine kinase: exploitation for therapeutic gain. *Pharmacol Rev* 65 906–943. [PubMed: 23592612]
- Borea PA, Gessi S, Merighi S & Varani K 2016 Adenosine as a multi-signalling guardian angel in human diseases: When, where and how does it exert its protective effects? *Trends Pharmacol Sci* 37 419–434. [PubMed: 26944097]
- Bouma MG, van den Wildenberg FA & Buurman WA 1996 Adenosine inhibits cytokine release and expression of adhesion molecules by activated human endothelial cells. *Am J Physiol* 270 C522–C529. [PubMed: 8779915]
- Cook S, Hugli O, Egli M, Menard B, Thalmann S, Sartori C, Perrin C, Nicod P, Thorens B, Vollenweider P, et al. 2004 Partial gene deletion of endothelial nitric oxide synthase predisposes to exaggerated high-fat diet-induced insulin resistance and arterial hypertension. *Diabetes* 53 2067–2072. [PubMed: 15277387]
- Csoka B, Koscsó B, Toro G, Kokai E, Virag L, Nemeth ZH, Pacher P, Bai P & Hasko G 2014 A2B adenosine receptors prevent insulin resistance by inhibiting adipose tissue inflammation via maintaining alternative macrophage activation. *Diabetes* 63 850–866. [PubMed: 24194503]
- Du X, Ou X, Song T, Zhang W, Cong F, Zhang S & Xiong Y 2015 Adenosine A2B receptor stimulates angiogenesis by inducing VEGF and eNOS in human microvascular endothelial cells. *Exp Biol Med* 240 1472–1479.
- Duplain H, Burcelin R, Sartori C, Cook S, Egli M, Lepori M, Vollenweider P, Pedrazzini T, Nicod P, Thorens B, et al. 2001 Insulin resistance, hyperlipidemia, and hypertension in mice lacking endothelial nitric oxide synthase. *Circulation* 104 342–345. [PubMed: 11457755]

- Gogg S, Smith U & Jansson PA 2009 Increased MAPK activation and impaired insulin signaling in subcutaneous microvascular endothelial cells in type 2 diabetes: the role of endothelin-1. *Diabetes* 58 2238–2245. [PubMed: 19581418]
- Graupera M & Claret M 2018 Endothelial cells: new players in obesity and related metabolic disorders. *Trends Endocrinol Metab* 29 781–794. [PubMed: 30266200]
- Green A, Fisher M & Newsholme EA 1981 Maximum activities of enzymes involved in adenosine metabolism in adipose tissue of rats and mice under conditions of variations in insulin sensitivity. *Biochim Biophys Acta* 676 125–128. [PubMed: 6266499]
- Gustavo Vazquez-Jimenez J, Chavez-Reyes J, Romero-Garcia T, Zarain-Herzberg A, Valdes-Flores J, Manuel Galindo-Rosales J, Rueda A, Guerrero-Hernandez A & Olivares-Reyes JA 2016 Palmitic acid but not palmitoleic acid induces insulin resistance in a human endothelial cell line by decreasing SERCA pump expression. *Cell Signal* 28 53–59. [PubMed: 26475209]
- Handa P, Tateya S, Rizzo NO, Cheng AM, Morgan-Stevenson V, Han CY, Clowes AW, Daum G, O'Brien KD, Schwartz MW, et al. 2011 Reduced vascular nitric oxide-cGMP signaling contributes to adipose tissue inflammation during high-fat feeding. *Arterioscler Thromb Vasc Biol* 12 2827–2835.
- Hasegawa Y, Saito T, Ogihara T, Ishigaki Y, Yamada T, Imai J, Uno K, Gao J, Kaneko K, Shimosawa T, et al. 2012 Blockade of the nuclear factor-kappaB pathway in the endothelium prevents insulin resistance and prolongs life spans. *Circulation* 125 1122–1133. [PubMed: 22302838]
- Kashiwagi S, Atochin DN, Li Q, Schleicher M, Pong T, Sessa WC & Huang PL 2013 eNOS phosphorylation on serine 1176 affects insulin sensitivity and adiposity. *Biochem Biophys Res Commun* 2 284–290.
- Konishi M, Sakaguchi M, Lockhart SM, Cai W, Li ME, Homan EP, Rask-Madsen C & Kahn CR 2017 Endothelial insulin receptors differentially control insulin signaling kinetics in peripheral tissues and brain of mice. *Proc Natl Acad Sci U S A* 114 E8478–E8487. [PubMed: 28923931]
- Kubota T, Kubota N, Kumagai H, Yamaguchi S, Kozono H, Takahashi T, Inoue M, Itoh S, Takamoto I, Sasako T, et al. 2011 Impaired insulin signaling in endothelial cells reduces insulin-induced glucose uptake by skeletal muscle. *Cell Metab* 13 294–307. [PubMed: 21356519]
- Lee WJ, Tateya S, Cheng AM, Rizzo-DeLeon N, Wang NF, Handa P, Wilson CL, Clowes AW, Sweet IR, Bomsztyk K, et al. 2015 M2 macrophage polarization mediates anti-inflammatory effects of endothelial nitric oxide signaling. *Diabetes* 64 2836–2846. [PubMed: 25845662]
- Liu Z, Yan S, Wang J, Xu Y, Wang Y, Zhang S, Xu X, Yang Q, Zeng X, Zhou Y, et al. 2017 Endothelial adenosine A2a receptor-mediated glycolysis is essential for pathological retinal angiogenesis. *Nat Commun* 8 584. [PubMed: 28928465]
- Luan G, Gao Q, Guan Y, Zhai F, Zhou J, Liu C, Chen Y, Yao K, Qi X & Li T 2013 Upregulation of adenosine kinase in Rasmussen encephalitis. *J Neuropathol Exp Neurol* 72 1000–1008. [PubMed: 24128682]
- Maloney E, Sweet IR, Hockenbery DM, Pham M, Rizzo NO, Tateya S, Handa P, Schwartz MW & Kim F 2009 Activation of NF-kappaB by palmitate in endothelial cells: a key role for NADPH oxidase-derived superoxide in response to TLR4 activation. *Arterioscler Thromb Vasc Biol* 29 1370–1375. [PubMed: 19542021]
- Mather KJ, Steinberg HO & Baron AD 2013 Insulin resistance in the vasculature. *J Clin Invest* 123 1003–1004. [PubMed: 23454764]
- Navarro G, Abdolazimi Y, Zhao Z, Xu H, Lee S, Armstrong NA & Annes JP 2017 Genetic disruption of adenosine kinase in mouse pancreatic beta-cells protects against high-fat diet-induced glucose intolerance. *Diabetes* 66 1928–1938. [PubMed: 28468960]
- Pardo F, Villalobos-Labra R, Chiarello DI, Salsoso R, Toledo F, Gutierrez J, Leiva A & Sobrevia L 2017 Molecular implications of adenosine in obesity. *Mol Aspects Med* 55 90–101. [PubMed: 28104382]
- Pawelczyk T, Sakowicz M, Podgorska M & Szczepanska-Konkel M 2003 Insulin induces expression of adenosine kinase gene in rat lymphocytes by signaling through the mitogen-activated protein kinase pathway. *Exp Cell Res* 286 152–163. [PubMed: 12729803]
- Pi X, Xie L & Patterson C 2018 Emerging roles of vascular endothelium in metabolic homeostasis. *Circ Res* 123 477–494. [PubMed: 30355249]

- Pye C, Elsherbiny NM, Ibrahim AS, Liou GI, Chadli A, Al-Shabrawey M & Elmarakby AA 2014 Adenosine kinase inhibition protects the kidney against streptozotocin-induced diabetes through anti-inflammatory and anti-oxidant mechanisms. *Pharmacol Res* 85 45–54. [PubMed: 24841126]
- Seki T, Hosaka K, Fischer C, Lim S, Andersson P, Abe M, Iwamoto H, Gao Y, Wang X, Fong GH, et al. 2018 Ablation of endothelial VEGFR1 improves metabolic dysfunction by inducing adipose tissue browning. *J Exp Med* 215 611–626. [PubMed: 29305395]
- Smits P, Williams SB, Lipson DE, Banitt P, Rongen GA & Creager MA 1995 Endothelial release of nitric oxide contributes to the vasodilator effect of adenosine in humans. *Circulation* 92 2135–2141. [PubMed: 7554193]
- Wahlman C, Doyle TM, Little JW, Luongo L, Janes K, Chen Z, Esposito E, Tosh DK, Cuzzocrea S, Jacobson KA, et al. 2018 Chemotherapy-induced pain is promoted by enhanced spinal adenosine kinase levels through astrocyte-dependent mechanisms. *Pain* 159 1025–1034. [PubMed: 29419652]
- Xu Y, Wang Y, Yan S, Yang Q, Zhou Y, Zeng X, Liu Z, An X, Toque HA, Dong Z, et al. 2017a Regulation of endothelial intracellular adenosine via adenosine kinase epigenetically modulates vascular inflammation. *Nat Commun* 8 943. [PubMed: 29038540]
- Xu Y, Wang Y, Yan S, Zhou Y, Yang Q, Pan Y, Zeng X, An X, Liu Z, Wang L, et al. 2017b Intracellular adenosine regulates epigenetic programming in endothelial cells to promote angiogenesis. *EMBO Mol Med* 9 1263–1278. [PubMed: 28751580]
- Xue Y, Lim S, Brakenhielm E & Cao Y 2010 Adipose angiogenesis: quantitative methods to study microvessel growth, regression and remodeling in vivo. *Nat Protoc* 5 912–920. [PubMed: 20431536]
- Yokoyama M, Okada S, Nakagomi A, Moriya J, Shimizu I, Nojima A, Yoshida Y, Ichimiya H, Kamimura N, Kobayashi Y, et al. 2014 Inhibition of endothelial p53 improves metabolic abnormalities related to dietary obesity. *Cell Rep* 7 1691–1703. [PubMed: 24857662]

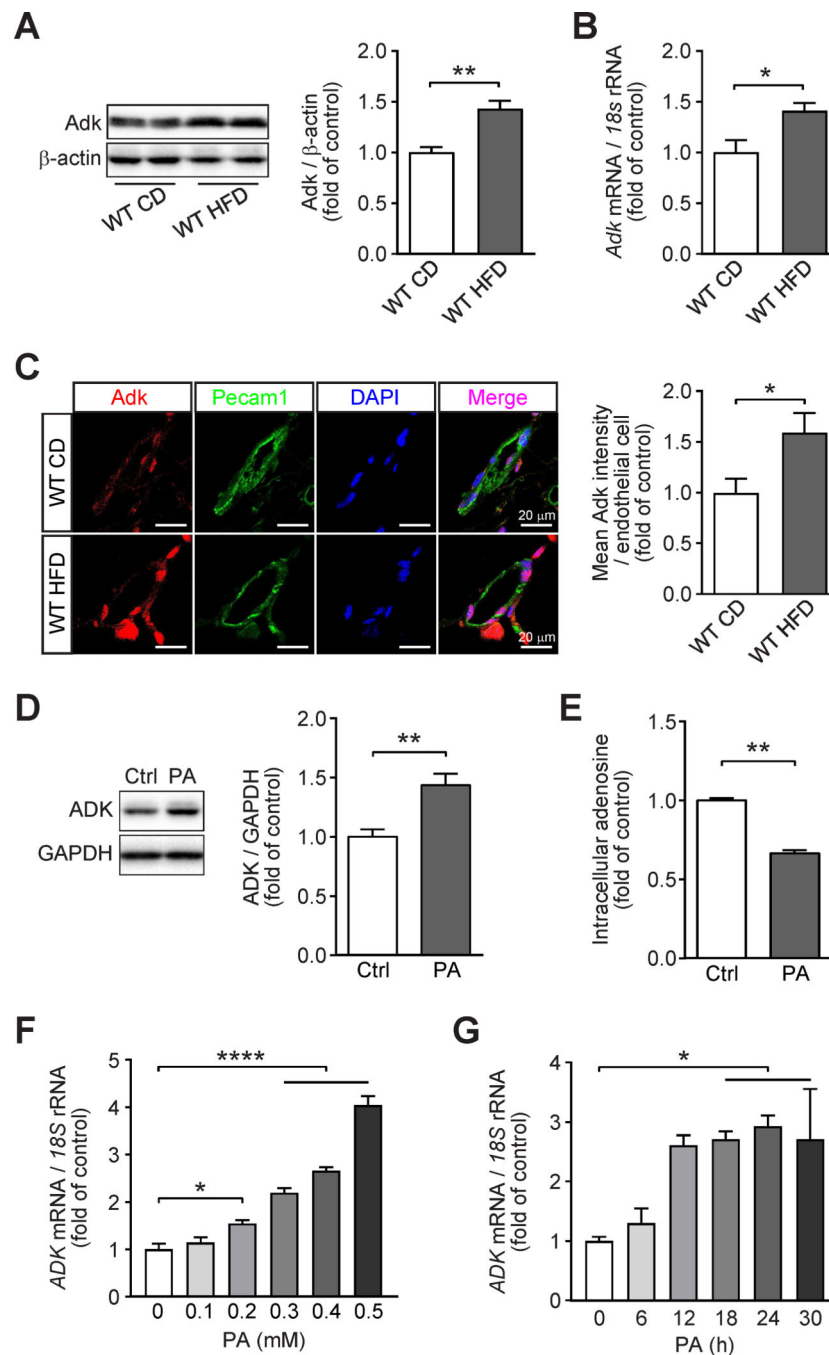


Figure 1. Increased expression of endothelial adenosine kinase (ADK) in diet-induced obese mice and endothelial cells treated with palmitic acid (PA).

A. Representative Western blot results of Adk and β -actin (left) in adipose tissue from wild-type (WT) mice fed either a chow diet (CD) or a high-fat diet (HFD) for 12 weeks starting at 6-week-age and relative ratio of Adk/ β -actin (right) were quantitated by densitometric analysis of the corresponding Western blots (n = 4). **B.** qPCR analysis of *Adk* expression in adipose tissue from wild-type (WT) mice fed either a chow diet (CD) or a high-fat diet (HFD) for 12 weeks starting at 6-week-age (n = 5). **C.** Representative images (left) and

quantification (right) of immunofluorescence staining for Adk in adipose vessels from wild-type (WT) mice fed either a chow diet (CD) or a high-fat diet (HFD) for 12 weeks starting at 6-week-age (n = 4). **D.** Representative Western blot results of ADK and GAPDH in HUVECs treated with PA at 0.4 mM for 24 h (left) and relative ratio of ADK/GAPDH (right) were quantitated by densitometric analysis of the corresponding Western blots (n = 5). **E.** Quantification of relative intracellular adenosine concentration in HUVECs treated with vehicle (Ctrl) or PA (0.4 mM) for 24 h (n = 4). **F.** qPCR analysis of *ADK* expression in HUVECs treated with increasing concentrations of PA (0.1–0.5 mM) for 24 h (n = 4). **G.** qPCR analysis of ADK expression in HUVECs treated with PA (0.4mM) for the indicated times (n = 3). All data are represented as mean \pm SEM, * $P < 0.05$, ** $P < 0.01$ and **** $P < 0.0001$ for indicated comparisons; unpaired two-tailed Student's *t* test for (A-E); one-way ANOVA with Bonferroni's post-hoc test for (F and G).

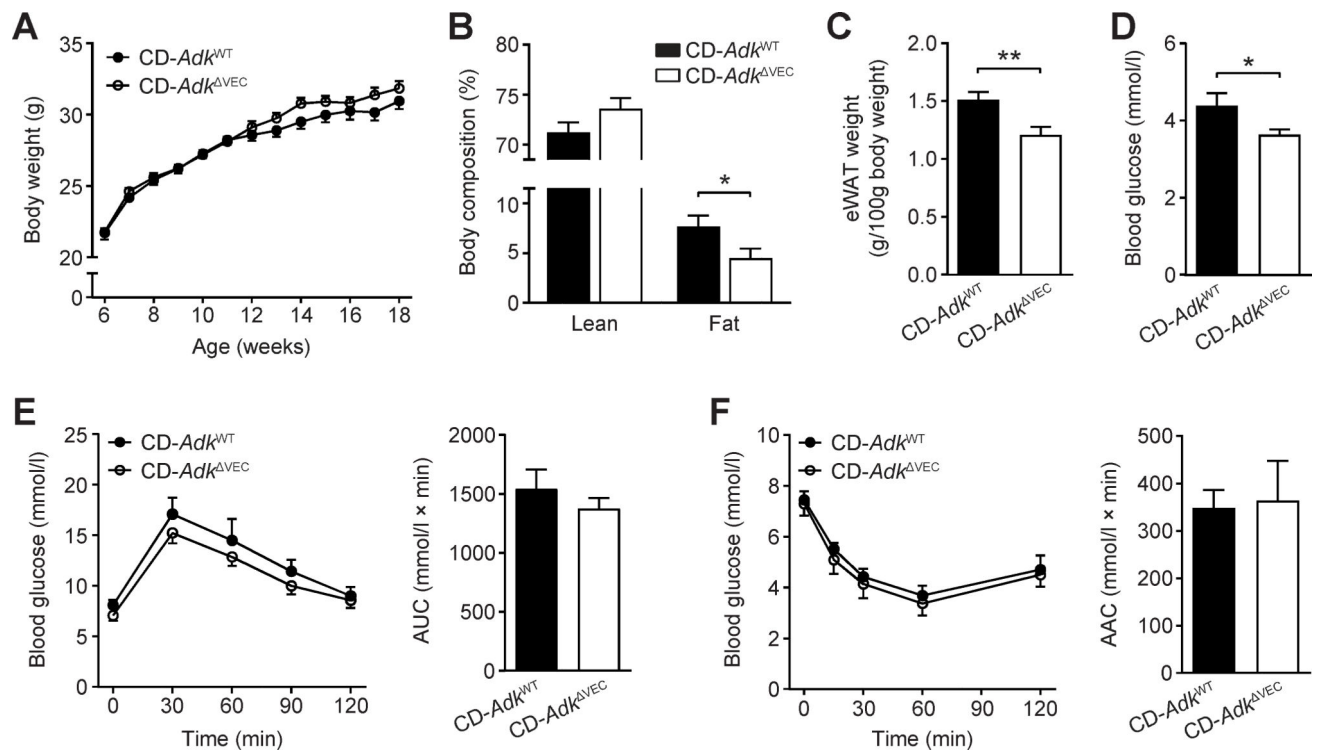


Figure 2. Body mass and glucose homeostasis of the EC *Adk*-deficient mice on a chow diet (CD). **A.** Body weight of *Adk*^{WT} and *Adk*^{ΔVEC} mice at the indicated age (n = 9–10 mice per group). **B.** Lean and fat content of *Adk*^{WT} and *Adk*^{ΔVEC} mice at the age of 14 weeks (n = 8 mice per group). **C.** The weight of epididymal WAT (eWAT) in *Adk*^{WT} and *Adk*^{ΔVEC} mice at the age of 14 weeks (n = 15–17 mice per group). **D.** Fasting blood glucose levels of *Adk*^{WT} and *Adk*^{ΔVEC} mice at the age of 14 weeks (n = 7–13 mice per group). **E.** Blood glucose levels (left) and AUC (area under the curve, right) during GTT (glucose tolerance test) in *Adk*^{WT} and *Adk*^{ΔVEC} mice at the age of 16 weeks (n = 6 mice per group). Mice were fasted for 6 h and injected with glucose (2 g/kg i.p.). **F.** Blood glucose levels (left) and AAC (area above the curve, right) during ITT (insulin tolerance test) in *Adk*^{WT} and *Adk*^{ΔVEC} mice at the age of 17 weeks (n = 5–6 mice per group). Mice were fasted for 4 h and injected with insulin (1 unit/kg i.p.). All data are represented as mean ± SEM, **P* < 0.05 and ***P* < 0.01 for *Adk*^{ΔVEC} vs. *Adk*^{WT} (unpaired two-tailed Student's *t* test).

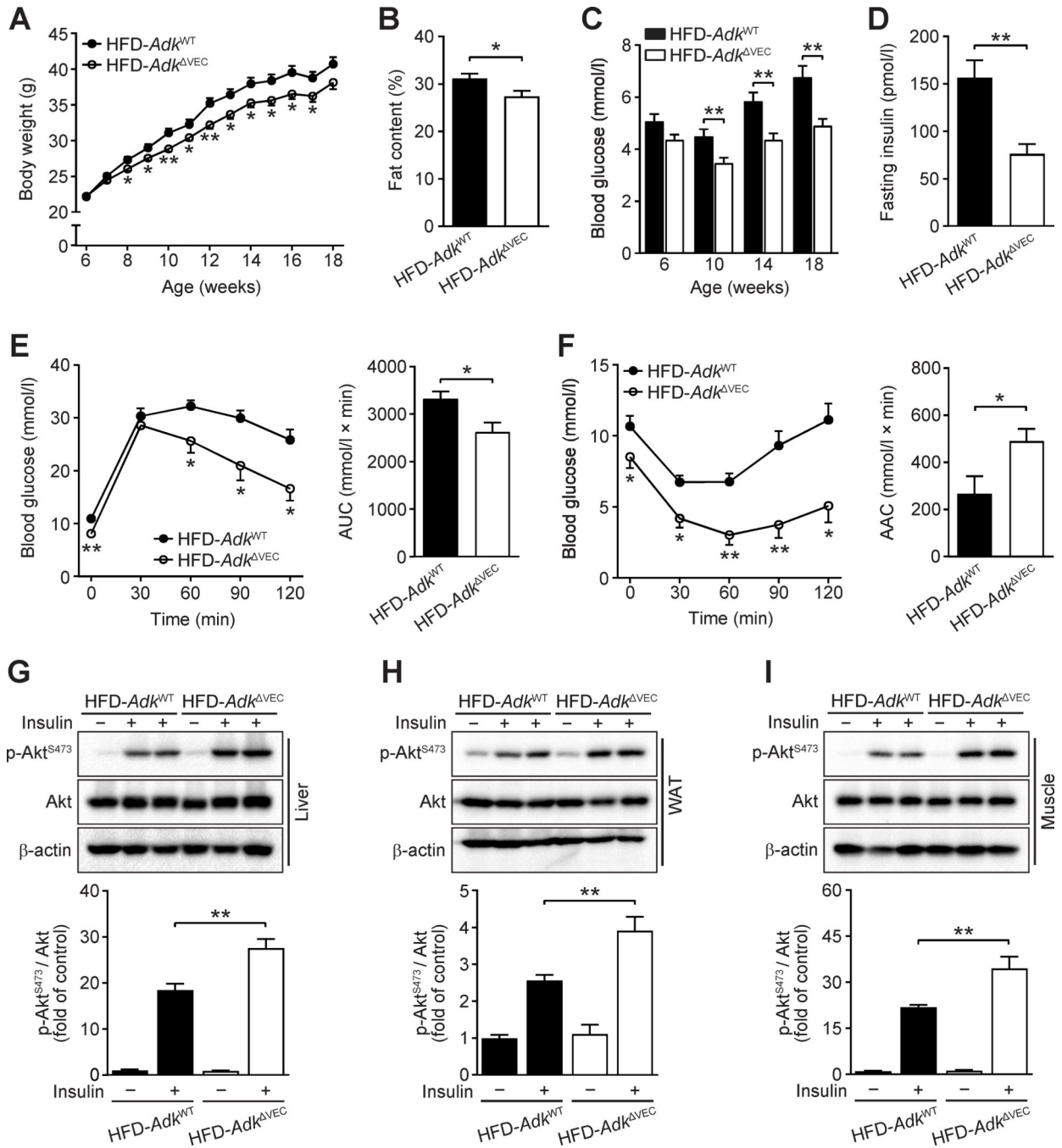


Figure 3. Improved HFD-induced systemic insulin sensitivity in EC *Adk*-deficient mice.

A. Body weight of *Adk*^{WT} and *Adk*^{ΔVEC} mice during 12 weeks of HFD (n = 10 mice per group). **B.** Fat content of *Adk*^{WT} and *Adk*^{ΔVEC} mice after 12 weeks of HFD (n = 10 mice per group). **C.** Fasting blood glucose levels of *Adk*^{WT} and *Adk*^{ΔVEC} mice during 12 weeks of HFD (n = 10 mice per group). **D.** Fasting serum insulin levels of *Adk*^{WT} and *Adk*^{ΔVEC} mice after 12 weeks of HFD (n = 10 mice per group). **E.** Blood glucose levels (left) and AUC (area under the curve, right) during GTT (glucose tolerance test) in *Adk*^{WT} and *Adk*^{ΔVEC} mice after 10 weeks of HFD (n = 6 mice per group). Mice were fasted for 6 h and

injected with glucose (2 g/kg i.p.). **F.** Blood glucose levels (left) and AAC (area above the curve, right) during ITT (insulin tolerance test) in *Adk*^{WT} and *Adk*^{VEC} mice after 11 weeks of HFD (n = 6 mice per group). Mice were fasted for 4 h and injected with insulin (0.75 unit/kg i.p.). **G-I.** Representative Western blot results of phospho-Akt (Ser473) (p-Akt^{S473}), total Akt (Akt) and β -actin from liver (G, top), epididymal WAT (H, top) and quadriceps muscle (I, top) in *Adk*^{WT} and *Adk*^{VEC} mice after 12 weeks of HFD. Samples were collected 5 min after mice were injected with saline or insulin (1 units/kg) into the inferior vena cava. Relative ratio of p-Akt^{S473}/Akt in liver (G, bottom), epididymal WAT (H, bottom) and skeletal muscle (I, bottom) were quantitated by densitometric analysis of the corresponding Western blots (n = 6 mice per group). All data are represented as mean \pm SEM, **P* < 0.05 and ***P* < 0.01 for *Adk*^{VEC} vs. *Adk*^{WT} (unpaired two-tailed Student's *t* test).

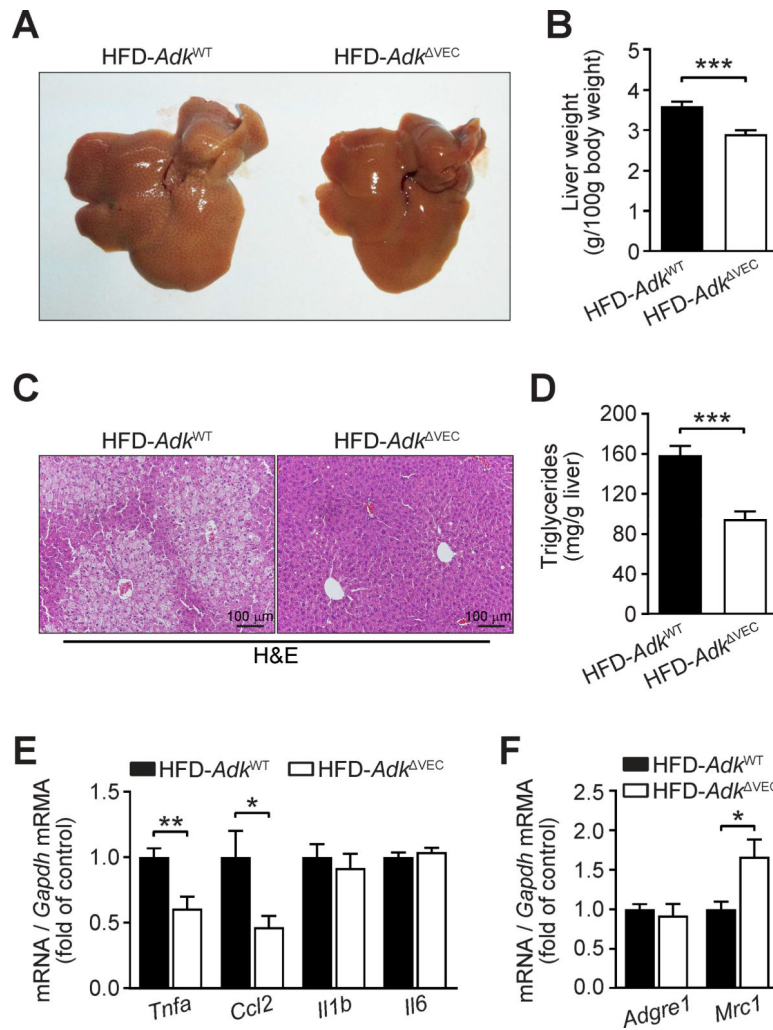


Figure 4. Decreased HFD-induced hepatic steatosis in EC *Adk*-deficient mice.

A. Representative gross morphology of liver from *Adk*^{WT} and *Adk*^{VEC} mice after 12 weeks of HFD (n = 4 images per group). **B.** Liver weight of *Adk*^{WT} and *Adk*^{VEC} mice after 12 weeks of HFD (n = 10 mice per group). **C.** Representative hematoxylin and eosin (H&E) staining of liver sections from *Adk*^{WT} and *Adk*^{VEC} mice after 12 weeks of HFD (n = 4 images per mouse; n = 4 mice per group). **D.** Triglyceride content in liver of *Adk*^{WT} and *Adk*^{VEC} mice after 12 weeks of HFD (n = 6 mice per group). **E.** qPCR analysis of expression of hepatic inflammatory cytokines in *Adk*^{WT} and *Adk*^{VEC} mice after 12 weeks of HFD (n = 8 mice per group). **F.** qPCR analysis of expression of hepatic M2 macrophage marker in *Adk*^{WT} and *Adk*^{VEC} mice after 12 weeks of HFD (n = 8 mice per group). All data are represented as mean ± SEM, **P* < 0.05, ***P* < 0.01 and ****P* < 0.001 for *Adk*^{VEC} vs. *Adk*^{WT} (unpaired two-tailed Student's *t* test).

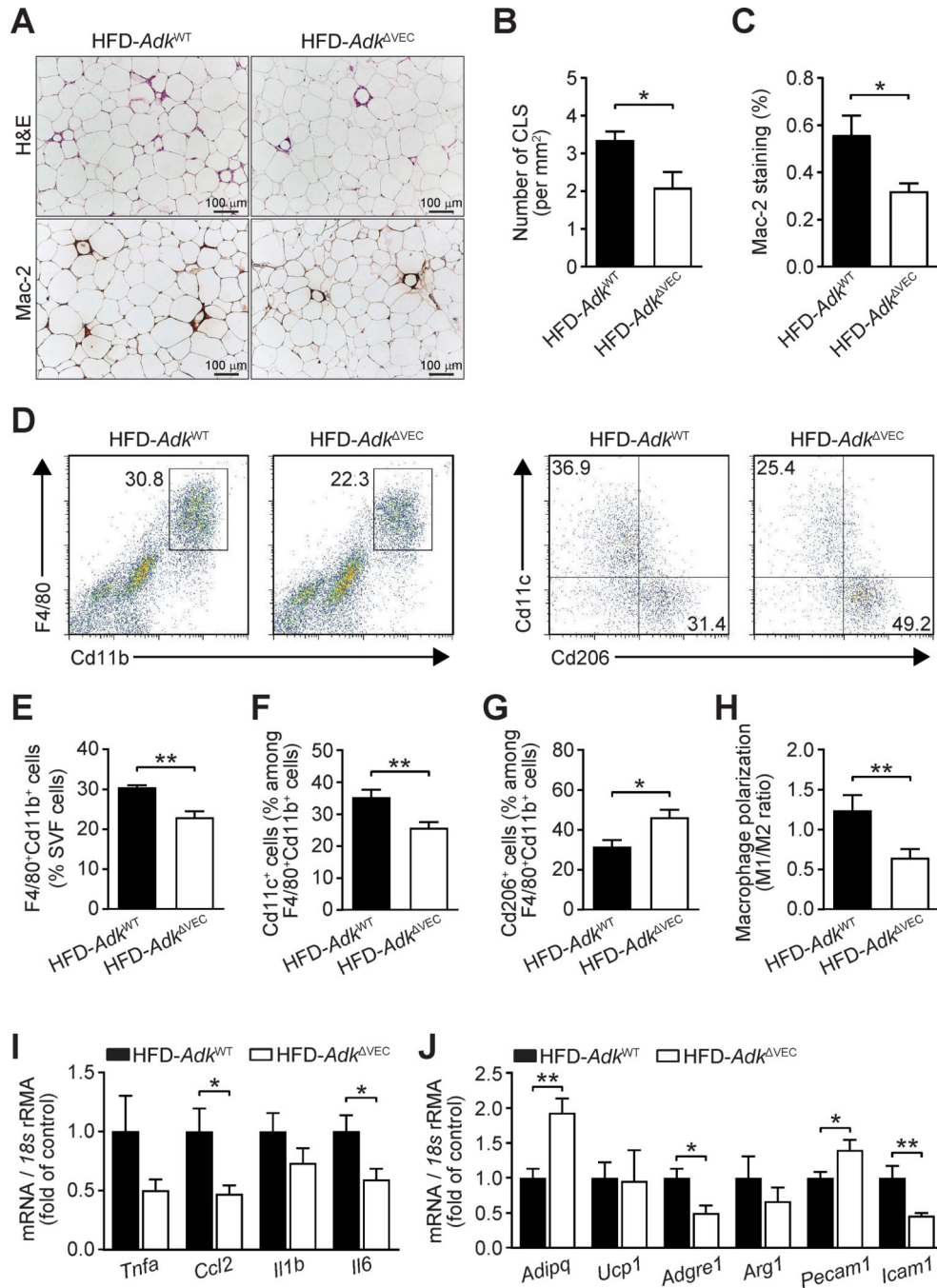


Figure 5. Decreased HFD-induced adipose inflammation in EC *Adk*-deficient mice.

A-C. Representative images of hematoxylin and eosin (H&E) staining (A, top) and Mac-2 immunohistochemical staining (A, bottom) and quantification of CLS (crown-like structure) numbers (B) from H&E staining and macrophage infiltration (C) from Mac-2 staining in epididymal WAT sections from *Adk*^{WT} and *Adk*^{VEC} mice after 12 weeks of HFD. (n = 4 mice per group). **D-J.** Representative flow cytometry plots and quantitative scatter plots showing percentage of Cd11b⁺F4/80⁺Cd11c⁺ (M1) macrophages (D, right and F), percentage of Cd11b⁺F4/80⁺Cd206⁺ (M2) macrophages (D, right and G), macrophage

polarization (H, M1/M2 ratio) and percentage of Cd11b⁺F4/80⁺ cells among stromal vascular fraction (SVF) cells (D, left and E) isolated from epididymal WAT of *Adk*^{WT} and *Adk*^{VEC} mice after 12 weeks of HFD (n = 8–12 mice per group). **I.** qPCR analysis of expression of inflammatory cytokines in epididymal WAT of *Adk*^{WT} and *Adk*^{VEC} mice after 12 weeks of HFD (n = 8 mice per group). **J.** qPCR analysis of expression of adipose tissue functional genes in epididymal WAT of *Adk*^{WT} and *Adk*^{VEC} mice after 12 weeks of HFD (n = 8 mice per group). All data are represented as mean ± SEM, **P* < 0.05 and ***P* < 0.01, for *Adk*^{VEC} vs. *Adk*^{WT} (unpaired two-tailed Student's *t* test).

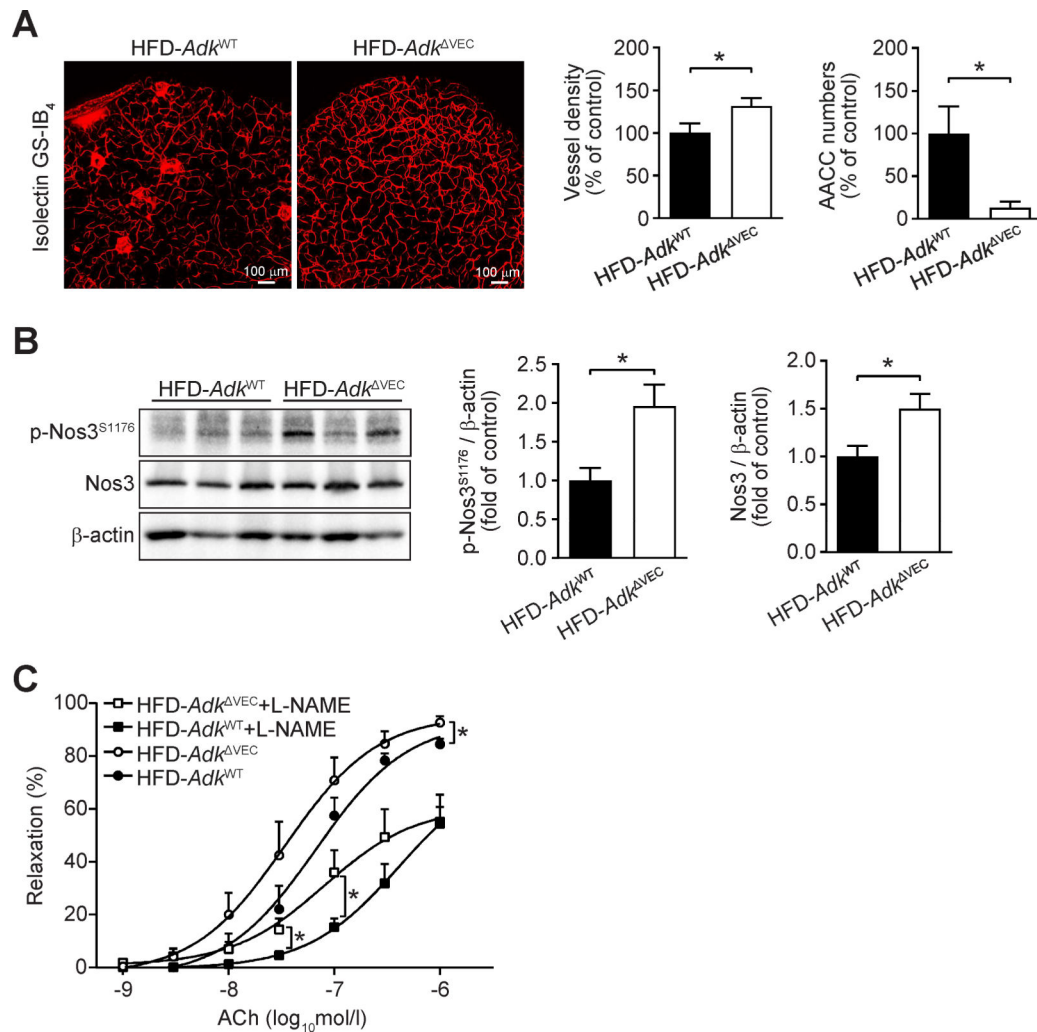


Figure 6. Improved HFD-induced endothelial dysfunction in EC Adk-deficient mice.

A. Representative images of immunofluorescence staining for isolectin GS-IB₄ (left) and quantification of vessel density (middle) and AACC (adipogenic/angiogenic cell cluster) numbers (right) in epididymal WAT from *Adk*^{WT} and *Adk*^{ΔVEC} mice after 12 weeks of HFD (n = 8 mice per group). **B.** Representative Western blot results of phospho-Nos3 (Ser1176) (p-Nos3^{S1176}), total Nos3 (Nos3) and β-actin (left) from epididymal WAT in *Adk*^{WT} and *Adk*^{ΔVEC} mice after 12 weeks of HFD. Relative ratio of p-Nos3^{S1176}/β-actin (middle) and Nos3/β-actin (right) in epididymal WAT were quantitated by densitometric analysis of the corresponding Western blots (n = 6 mice per group). **C.** Relaxations of skeletal muscle arterioles in response to cumulative concentrations of acetylcholine (ACh) in the absence or presence of N ω -nitro-L-arginine methyl ester hydrochloride (L-NAME). Arterioles were isolated from *Adk*^{WT} and *Adk*^{ΔVEC} mice after 12 weeks of HFD (n = 5–7 mice per group). All data are represented as mean \pm SEM, **P* < 0.05 and ***P* < 0.01 for *Adk*^{ΔVEC} vs. *Adk*^{WT} (unpaired two-tailed Student's *t* test).

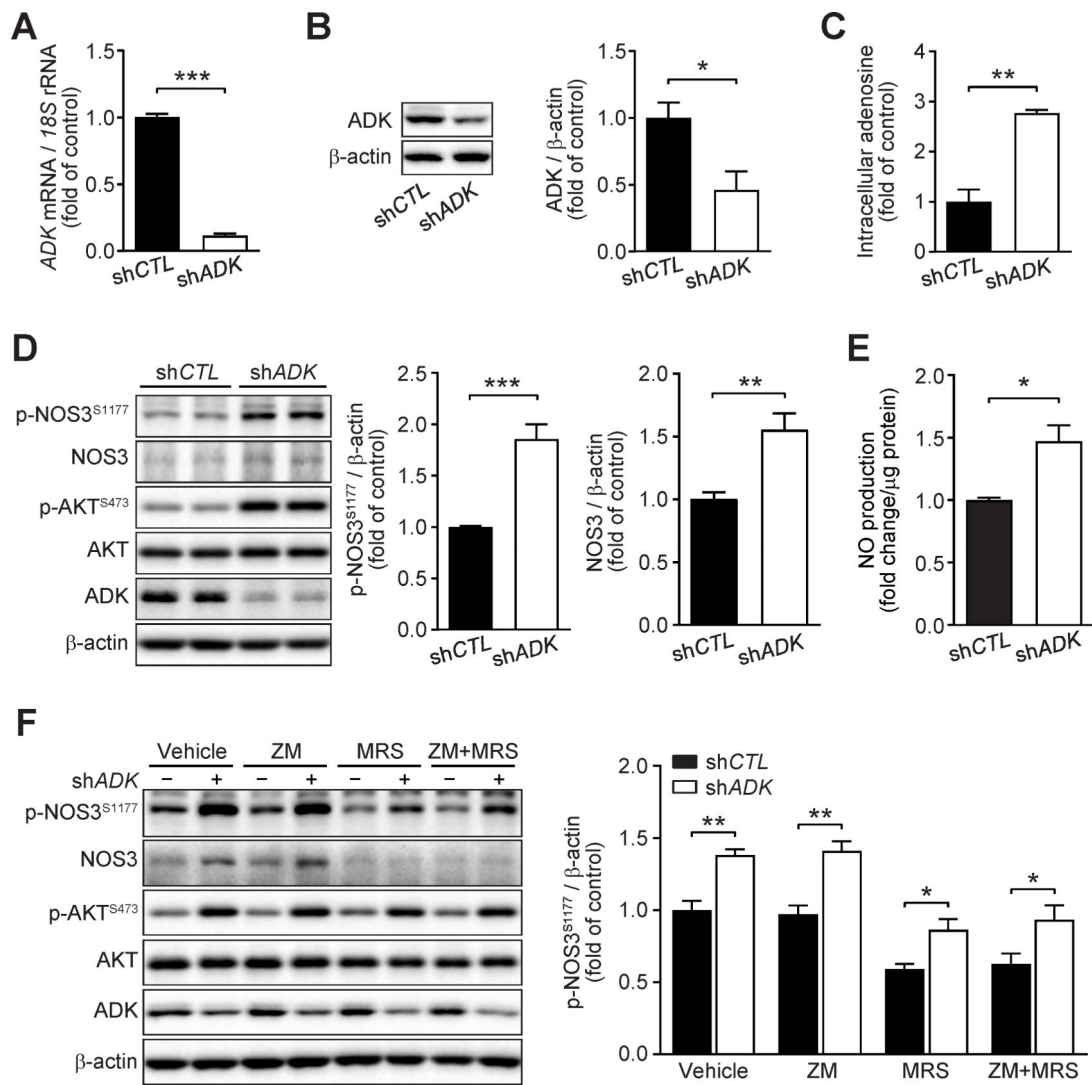


Figure 7. Increased endothelial nitric oxide synthase (NOS3)/nitric oxide (NO) pathway in ADK knockdown endothelial cells.

A. qPCR analysis of adenosine kinase (*ADK*) expression in human umbilical vein endothelial cells (HUVECs) infected with control shRNA (shCTL) or ADK shRNA (shADK) adenovirus for 48 h (n = 6). **B.** Representative Western blot results of ADK and β -actin in HUVECs infected with shCTL or shADK adenovirus for 48 h (left) and relative ratio of ADK/ β -actin (right) were quantitated by densitometric analysis of the corresponding Western blots (n = 3). **C.** Quantification of relative intracellular adenosine concentration in control (shCTL) and ADK knockdown (shADK) HUVECs (n = 3). **D.** Representative Western blot results of phospho-NOS3 (Ser1177) (p-NOS3^{S1177}), total NOS3 (NOS3), phospho-AKT (Ser473) (p-AKT^{S473}), total AKT (AKT), ADK and β -actin in HUVECs infected with shCTL or shADK adenovirus for 48 h (left) and relative ratio of p-NOS3^{S1177}/ β -actin (middle) and NOS3/ β -actin (right) were quantitated by densitometric analysis of the corresponding Western blots (n = 6). **E.** Quantification of relative NO concentration in the culture medium of HUVECs infected with control shRNA (shCTL) or ADK shRNA (shADK) adenovirus for 48 h (n = 4). **F.** Representative Western blot results of endothelial

phospho-NOS3 (Ser1177) (p-NOS3^{S1177}), total NOS3 (NOS3), phospho-AKT (Ser473) (p-AKT^{S473}), total AKT (AKT), ADK and β -actin (left). HUVECs were infected with sh*CTL* or sh*ADK* adenovirus for 24 h, then treated with ZM 241385 (5 μ M), MRS 1754 (5 μ M) or both ZM 241385 and MRS 1754 for another 24 h. Relative ratio of p- NOS3^{S1177}/ β -actin (right) were quantitated by densitometric analysis of the corresponding Western blots (n = 4). All data are represented as mean \pm SEM, * P < 0.05, ** P < 0.01 and *** P < 0.001 for indicated comparisons (unpaired two-tailed Student's t test).

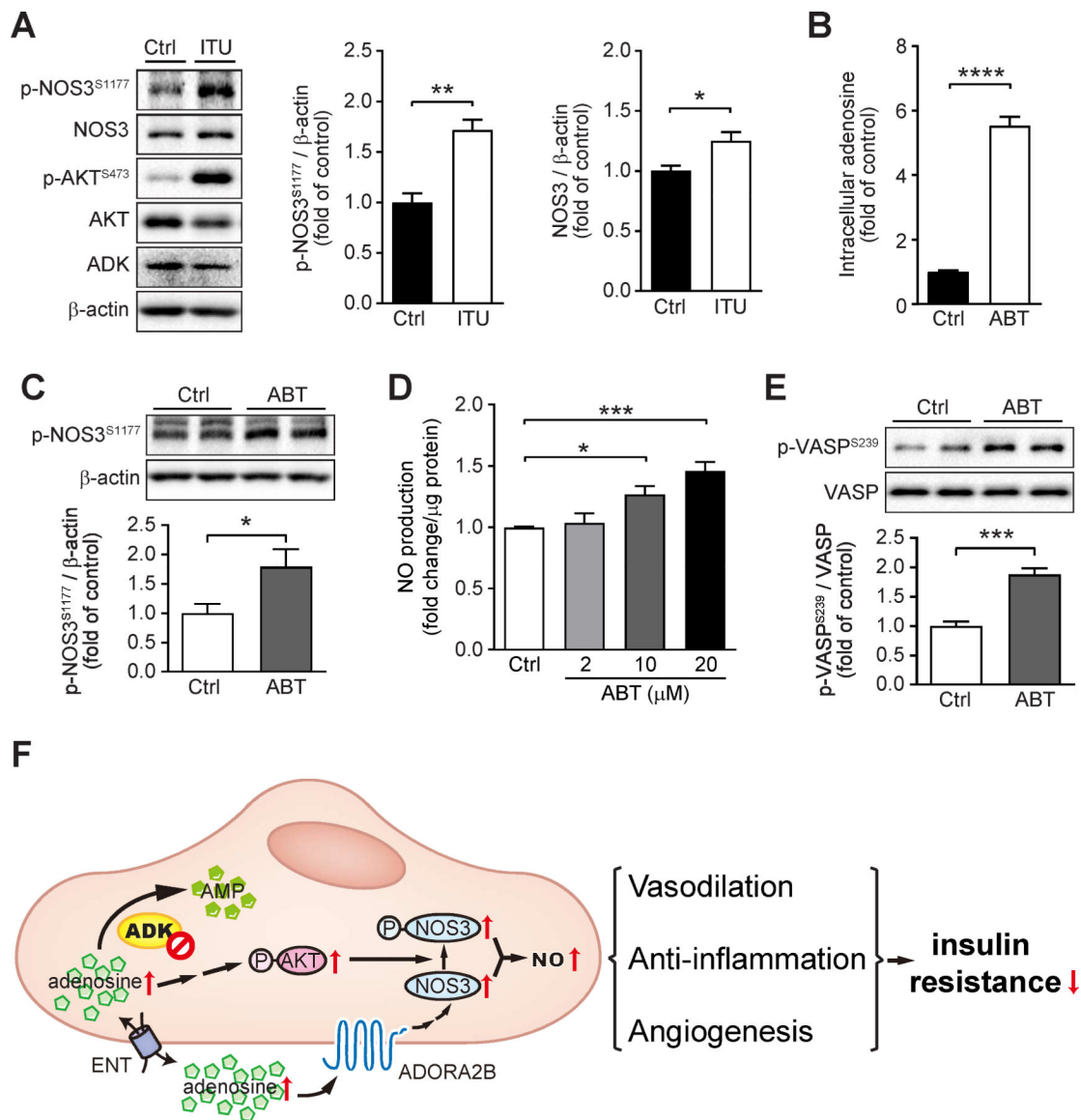


Figure 8. Increased endothelial nitric oxide synthase (NOS3)/nitric oxide (NO) pathway in endothelial cells treated with ADK inhibitors

A. Representative Western blot results of phospho-NOS3 (Ser1177) (p-NOS3^{S1177}), total NOS3 (NOS3), phospho-AKT (Ser473) (p-AKT^{S473}), total AKT (AKT), ADK and β-actin in HUVECs (human umbilical vein endothelial cells) treated with vehicle (Ctrl) and ITU (10 μM) for 4 h (left), and relative ratio of p-NOS3^{S1177}/β-actin (right) were quantitated by densitometric analysis of the corresponding Western blots (n = 3). **B.** Quantification of relative intracellular adenosine concentration in HUVECs treated with vehicle (Ctrl) and ABT702 (ABT) (10 μM) for 6 h (n = 6). **C.** Representative Western blot results of phospho-NOS3 (Ser1177) (p-NOS3^{S1177}) and β-actin in HUVECs treated with ABT at 10 μM for 24 h (top) and relative ratio of p-NOS3^{S1177}/β-actin were quantitated by densitometric analysis of the corresponding Western blots (bottom) (n = 5). **D.** Quantification of relative NO concentration in the culture medium of HUVECs treated with increasing concentrations of ABT (2–20 μM) for 24 h (n = 6). **E.** Representative Western blot results of phospho-VASP

(Ser239) (p-VASP^{S239}) and total VASP (VASP) in HUVECs treated with ABT at 10 μ M for 24 h (top) and relative ratio of p-VASP^{S239}/VASP were quantitated by densitometric analysis of the corresponding Western blots (bottom) (n = 4). Data (A-E) are represented as mean \pm SEM, * P < 0.05, ** P < 0.01, *** P < 0.001 and **** P < 0.001 for indicated comparisons; unpaired two-tailed Student's t test for (A-C and E), one-way ANOVA with Bonferroni's post-hoc test for (D). F. Schematic of the proposed mechanism for endothelial ADK deficiency-mediated improved insulin sensitivity. Increased NOS3 activity in ADK deficient ECs is achieved through adenosine receptor A2b -dependent NOS3 protein upregulation and p-AKT/p-NOS3 dependent NOS3 activation. Elevated NO production protects mice from diet-induced insulin resistance through vasodilation, anti-inflammation and angiogenesis. AMP, adenosine monophosphate; ADK, adenosine kinase; ENT, equilibrative nucleoside transporter; ADORA2B, adenosine receptor A2b; p-NOS3, phospho-NOS3 (Ser1177); p-AKT, phospho-AKT (Ser473); NO, nitric oxide.